Chinese Chemical Letters 35 (2024) 108506

Contents lists available at ScienceDirect

Chinese Chemical Letters

journal homepage: www.elsevier.com/locate/cclet

A nanoagent for concurrent therapy of breast cancer bone metastasis and cancer-induced bone pain through SLC7A11 interruption and photodynamic therapy

Qi Fu[a], Zhongming Lian[a], Mengya Niu[b], Yaru Huang[a], Yanqiu Ai[a], Long He[a], Dandan Zhang[b], Cuixia Zheng[c], Jian-Jun Yang[a,*], Lei Wang[b,d,*], Dandan Tian[a,*]

[a] *Department of Anesthesiology, Pain and Perioperative Medicine, The First Affiliated Hospital of Zhengzhou University, Zhengzhou 450001, China*
[b] *School of Pharmaceutical Sciences, Zhengzhou University, Zhengzhou 450001, China*
[c] *Translational Medical Center of Huaihe Hospital, Henan University, Kaifeng 475004, China*
[d] *Key Laboratory of Advanced Drug Preparation Technologies, Ministry of Education, School of Pharmaceutical Sciences, Zhengzhou University, Zhengzhou 450001, China*

ARTICLE INFO

Article history:
Received 9 March 2023
Revised 20 April 2023
Accepted 23 April 2023
Available online 27 April 2023

Keywords:
Breast cancer bone metastasis
Cancer-induced bone pain
Cystine/glutamate antiporter
Sorafenib
Photodynamic therapy

ABSTRACT

Bone metastasis, a life-threatening complication of advanced breast cancer, is often accompanied by debilitating pain (cancer-induced bone pain, CIBP) that severely impairs life quality and survival. The concurrent treatment of bone metastases and CIBP remains a clinical challenge because the therapeutic options are limited. In this study, we construct a near-infrared light-activated nano-therapeutic system to meet this conundrum. In detail, sorafenib (SRF) and photosensitizer (chlorin e6, Ce6) are encapsulated into mesoporous hydroxyapatite nanoparticles (HANPs), which are further functionalized with hyaluronic acid (HA) to obtain HA-SRF/Ce6@HANPs system. The designed nanoplatform destroys tumor cells *in vitro* and *in vivo via* the synergism of SRF (interrupting the exchange of cystine/glutamate by inhibiting SLC7A11) and photodynamic therapy (PDT, inducing reactive oxygen species generation). The decrease in tumor burden and reduction of extracellular glutamate significantly attenuate CIBP in mice model with developing bone cancer. Moreover, the combination of HA-SRF/Ce6@HANPs and PDT inhibit osteoclasts activation, promote osteoblast differentiation and accelerate bone repair. Overall, the nanoagent with good biocompatibility may provide an effective therapy method for the concurrent treatment of breast cancer bone metastasis and CIBP.

Although major breakthrough has been made in the fight against breast cancer, it remains the leading cause of death in women worldwide [1]. Around 70% of patients with breast cancer have had skeletal metastasis [2,3]. The patients suffer from life-threatening skeletal-related events, such as severe pain [4,5]. Most worthy of attention is that cancer-induced bone pain (CIBP) is not just the outcome of cancer, but a promoter of tumor progression [6,7]. Pain relief and cancer treatment are supplements for each other, indicating that concurrent therapy of cancer and CIBP makes sense in improving the efficacy of cancer comprehensive treatment [8].

Currently, CIBP management strategies focus on radiotherapy and analgesic drugs following three-step analgesic ladder [9,10]. However, system administration of these analgesic drugs is often accompanied by severe side effects [8]. It has been revealed that CIBP is a complex state with peripheral and central features containing multiple potential mechanisms [11,12]. On one hand, tumor and stromal cells can induce bone pain by disrupting host bone cell processes [13]. On the other hand, glutamate, a neurotransmitter released by cancer cells *via* the cystine/glutamate antiporter solute carrier family 7 member 11 (SLC7A11), is capable of initiating a pain response in peripheral tissues [14,15]. Therefore, inhibition of the SLC7A11 could alleviate CIBP by reducing glutamate release [16,17].

Coincidentally, SLC7A11 is important for cancer cells to maintain redox homeostasis by supplying cystine (oxidized cysteine) for glutathione (GSH) biosynthesis [18,19]. As the cofactor of glutathione peroxidase 4 (GPX4), GSH plays a key role in scavenging reactive oxygen species (ROS) and protecting cancer cells from oxidative damage [20]. Therefore, SLC7A11/GSH/GPX4 axis is the

* Corresponding authors.
E-mail addresses: jianjunyang1971@163.com (J.-J. Yang), wanglei1@zzu.edu.cn (L. Wang), ddt0802@163.com (D. Tian).

https://doi.org/10.1016/j.cclet.2023.108506
1001-8417/

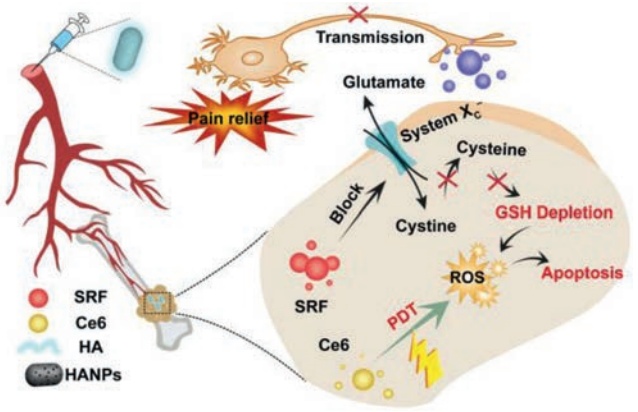

Scheme 1. Illustration of antitumor and analgesic effects of HA-SRF/Ce6@HANPs.

most important antioxidant system in many tumor types [21,22]. It has been reported that cystine-starved cells undergo imbalance of oxidative stress and sensitive to photodynamic therapy (PDT) [23,24]. Yet, deletion of SLC7A11 might be a feasible target to access to effective photodynamic strategies, being regarded as preeminent protocols for the treatment of breast cancer bone metastasis [25,26]. Preclinical and clinical research has discovered that sorafenib (SRF) could block the SLC7A11, suspend the transportation of cysteine and depress the production of GSH, thus it might be an ideal candidate to destroy aggressive cancer cells and mitigate CIBP [27,28].

Herein, sorafenib (SRF) and chlorin e6 (Ce6) were encapsulated into mesoporous hydroxyapatite nanoparticles (HANPs), and then the obtained SRF/Ce6@HANPs were capped with hyaluronic acid (HA) to construct HA-SRF/Ce6@HANPs system for concurrent cancer treatment and pain management. In the guidance of HA, HA-SRF/Ce6@HANPs could precisely accumulate in bone metastases. As shown in Scheme 1, the combination of HA-SRF/Ce6@HANPs and PDT, triggered by 660 nm laser irradiation, synergistically inhibited breast cancer growth both *in vitro* and *in vivo*. The decrease in tumor burden and reduction of extracellular glutamate significantly attenuated CIBP-associated flinching and other pain-related behaviors in mice model with developing bone cancer. Concomitantly, the nanoplatform broke "vicious cycle" by suppressing activation of osteoclasts and apoptosis in cancer cells. Moreover, bone repair was accelerated with assistance of calcium released by HANPs. This nanoplatform provided some new insights on the concurrent therapy of breast cancer bone metastases and CIBP.

High acidity is a hallmark of tumor microenvironment (TME) of bone metastasis, and acid-responsive drug delivery nanoplatform is of critical [29]. Firstly, HANPs were prepared *via* chemical precipitation and hydrothermal method [30]. Transmission electron microscope (TEM) image in Fig. 1a demonstrated its mesoporous rod-like morphology with average diameter of ~118 nm which was coincided with the result of dynamic light scattering (Fig. S1 in Supporting information). Then, the porosity of HANPs was measured *via* N_2 adsorption-desorption isotherms. The results in Figs. 1b and c displayed that surface area and pore size were about 51.5405 ± 0.1214 m^2/g and 10.4392 nm, respectively. Furthermore, element distribution (Fig. S2 in Supporting information) in HANPs was investigated by energy dispersive X-ray (EDX), proving successful preparation of HANPs. X-ray diffractometer (XRD) pattern of HANPs was detected, and the result (Fig. S3 in Supporting information) showed that the diffraction pattern of single-phase hydroxyapatite was matched well with the joint committee on powder diffraction standards (JCPDS) card [31].

Subsequently, HA was graphed onto the surface of HANPs through amidation reaction, to obtain HA-HANPs. The analysis of fourier-transform infrared spectroscopy (FTIR) indicated that HA was connected to HANPs successfully (Fig. S4 in Supporting information). As shown in Fig. 1d, HANPs were obviously covered by HA polymers. Meanwhile, the particle size of HA-HANPs was slightly increased significantly (Fig. 1e), and the zeta potential was decrease from 1.51 ± 0.07 mV to -19.2 ± 0.75 mV (Fig. 1f). Then, grafting degree of HA was analyzed by thermogravimetric study. As shown in Fig. 1g, in region of 200–800 °C, HA-HANPs showed a weight loss of 20.86 wt% due to HA decomposition, and the graft ratio of HA was calculated to be approximately 18.94 wt%.

Next, ultraviolet-visible (UV-vis) spectrum was used to characterize the drugs loaded nanoplatform. As shown in Fig. 1h, SRF and Ce6 were successfully loaded in HANPs to obtain SRF/Ce6@HANPs with high drugs entrapment efficiency (SRF: ~88.5% and Ce6: ~82.1%). Acid sensitivity of HANPs moved us to investigate the drug release profile *in vitro*. Fig. 1i showed that both SRF release increased about 70% in acid buffer than that in neutral condition, and Ce6 release profile exhibited same trend. These results indicated that HA-SRF/Ce6@HANPs were acid response nanoplatform. Moreover, the nanoplatform exhibited good storage stability with no significant changes of particle size (Fig. S5 in Supporting information).

Then, we were inspired to investigate anti-tumor effect of the nanoagent on 4T1 breast cancer cells. As shown in Fig. 2a and Fig. S6 (Supporting information), cellular uptake amount of FITC in HA-FITC@HANPs was 1.5-folded higher than that in FITC@HANPs at 4 h, implying their specially targeting effect. Moreover, cell inhibition effect of HA-SRF/Ce6@HANPs on 4T1 tumor cells showed concentration dependent manner (Fig. 2b). In addition, cell apoptosis induced by the nanoplatform was detected by annexin V-FITC/PI kit. And the results in Fig. 2c and Fig. S7 (Supporting information) demonstrated that around 62% of cells were in apoptotic stage after treatment with HA-SRF/Ce6@HANPs+Laser, which was significantly higher than that in HA-SRF@HANPs and HA-Ce6@HANPs +Laser groups.

Subsequently, we investigated ROS-generating activity with 2′,7′-dichlorodihydrofluorescein diacetate (DCFH-DA) as indicator. Although cancer cells depending on high level of ROS to maintain their proliferation, no apparent green fluorescence could be observed in control group and HANPs treated tumor cells, as displayed in Fig. 2d and Fig. S8 (Supporting information), which was mostly due to high ability of antioxidant defense system. After disruption of the antioxidant defense system by blocking SLC7A11 with SRF, weak fluorescence was observed in HA-SRF@HANPs group. When combined with PDT, a large amount of ROS accumulated in cancer cells as exhibited by strong green fluorescence in HA-SRF/Ce6@HANPs+Laser treated group (Fig. 2d and Fig. S8).

We further investigated anti-tumor mechanism of the nanoplatform *via* some experiments. Fig. 2e and Fig. S9 (Supporting information) clarified that HA-SRF@HANPs and HA-SRF/Ce6@HANPs+Laser significantly inhibited SLC7A11 expression, resulting in the disruption of cysteine metabolism homeostasis in tumor cells. Distribution of cystine/glutamate exchange would reduce release of glutamate and uptake of cystine. As shown in Fig. 2f, media glutamate concentration was reduced around 0.5-fold after treatment with HA-SRF@HANPs and HA-SRF/Ce6@HANPs+Laser. Insufficient supply of cysteine would induce an anergic state of intracellular GSH (Fig. 2g). It was presumed that HA-Ce6/SRF@HANPs+Laser could deplete GSH in two aspects: First and foremost, SRF directly decreased GSH concentration by cutting off its precursor [32]. Second, ROS generation in PDT could diminish GSH to some extent. Interestingly, GSH depletion inactivated lipid peroxidation repair enzyme GPX4, which was measured through a cellular western blot and glutathione peroxidase assay kit. HA-Ce6@HANPs+Laser and HA-Ce6/SRF@HANPs+Laser could reduce both expression (Fig. 2h and

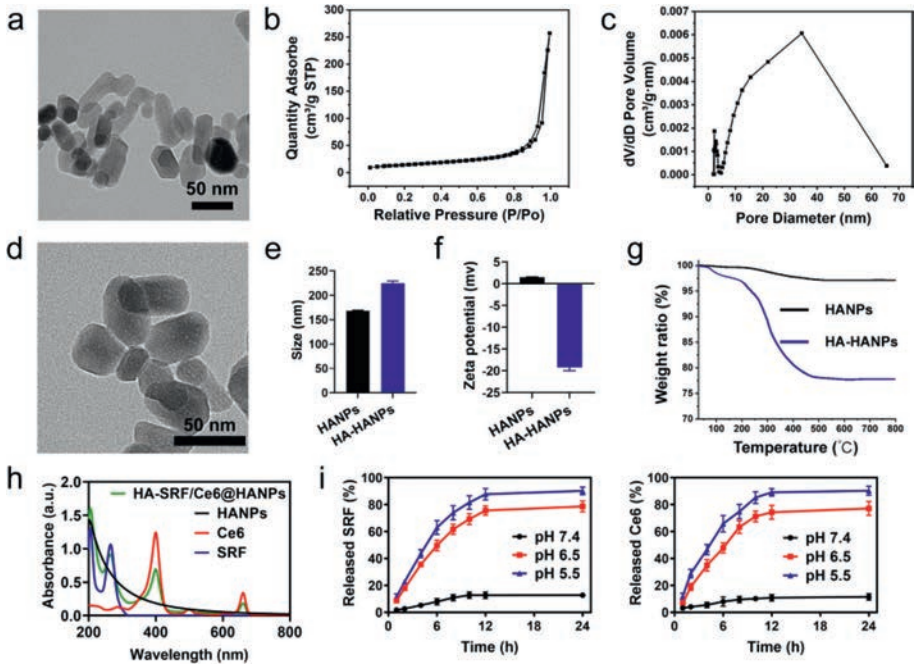

Fig. 1. (a) TEM of HANPs. (b, c) Nitrogen adsorption/desorption isotherms (b) and corresponding pore-size distribution curve of HANPs (c). (d) TEM of HA-HANPs. (e) Size distribution. (f) Zeta potential. (g) Thermogravimetric analysis. (h) UV–vis spectra. (i) Release profile of SRF and Ce6 from HA-SRF/Ce6@HANPs.

Fig. S10 in Supporting information) and activity (Fig 2i) of GPX4 in different degrees, which was consistent with the GSH depletion effect of the same group. Together, these experiments confirmed that HA-Ce6/SRF@HANPs+Laser could destroy the antioxidant system of tumor cells.

In light from above results, we were moved to investigate the *in vivo* antitumor effect on mouse model with bone metastasis. All animals were kept in a pathogen-free and well-fed environment. The procedures for care and use of animals were approved by the Ethics Committee of Zhengzhou University. Seven days post intratibial injection of 4T1 cells, the tumor-bearing mice were randomly divided into five groups and treated with different formulations *via* i.v. injections at equivalent SRF and Ce6 doses. As shown in Fig. 3a, HA-SRF@HANPs and HA-Ce6@HANPs+Laser inhibited tumor growth moderately after treatment for 18 days. In contrast, HA-Ce6/SRF@HANPs+Laser exhibited outstanding tumor inhibition efficiency, and these results were consistent with cytotoxicity *in vitro*. The mass of tumor concurred well with the tumor growth curve in the end of efficacy study (Fig. 3b). Then, main organs and tumor tissues were stained with the hematoxylin-eosin (H&E) staining, and tumor tissues were further stained with terminal deoxynucleotidyl transferase dUTP nick-end labeling (TUNEL) assay and Ki67.

As revealed in Fig. 3c, the tumor cells in control and HA-HANPs showed in highly aggressive shape of vigorous proliferation and closely arranged. The tumor cell morphologies treated with HA-SRF@HANPs and HA-Ce6@HANPs+Laser changed in varying degrees, while the mice treated with HA-Ce6/SRF@HANPs+Laser showed significant apoptosis and necrosis, demonstrating its highest potency in eradicating breast cancer bone metastases. Cell proliferation marker Ki67 was also significantly down-regulated after treatment with HA-Ce6/SRF@HANPs+Laser (Fig. 3d). Moreover, immunofluorescent images displayed a large number of TUNEL positive cells in HA-Ce6/SRF@HANPs+Laser group, which was significantly higher than that of HA-SRF@HANPs and HA-Ce6@HANPs+Laser groups (Fig. 3e).

After evaluation of anticancer effect, the inhibition effect of HA-Ce6@HANPs+Laser on osteolysis induced by bone metastasis was studied. Tartrate-resistant acid phosphatase (TRAP) is the biomarker for osteoclasts that reflect bone resorption *in vivo*. Immunohistochemical staining was used to analyze TRAP expression in bone microenvironment of tumor-bearing tibiae. After treatment with HA-SRF/Ce6@HANPs+Laser, TRAP-positive osteoclasts remarkably decreased in interface between tumor and bone compared with untreated group (Figs. 4a and b). Administration of HA-SRF@HANPs and HA-Ce6@HANPs+Laser only resulted in a minor reduction of TRAP-positive osteoclasts. The changes of TRAP in HA-SRF/Ce6@HANPs+Laser group demonstrated that bone resorption was significantly decreased.

CIBP is a frequent symptom of breast cancer patients with bone metastasis [33]. After administration with different formulations, pain behavior in tumor bearing mice was evaluated by recording the number of flinches, spontaneous lifting time and the movement scores of tumor-bearing limbs over a 4-min time period [34,35]. Spontaneous lifting of the tumor-bearing limb was first observed on Day 7 post-injection of breast cancer cells. Both the number of flinches and spontaneous lifting time gradually increased over time (Figs. 4c and d). Comparatively, HA-SRF@HANPs and HA-Ce6@HANPs+Laser could partially attenuated mice flinching compared to control group. Obvious difference of flinches number between control and HA-SRF/Ce6@HANPs+Laser groups was first observed on Day 9, and maximum difference was observed on Day 19. Moreover, the use of tumor bearing hindlimb was scored to evaluate pain level. As depicted in Fig. 4e, the use of tumor-bearing limb in HA-SRF/Ce6@HANPs+Laser group appeared normal with occasional limping. However, mice in control group showed partial or non-use of the tumor-bearing limb at the endpoint. All of the results suggested that HA-SRF/Ce6@HANPs+Laser could not only inhibit the tumor cells proliferation, but also inhibit osteoclasts activation and alleviate bone pain of bone metastatic mice, synergistically blocking vicious cycle of bone metastasis.

Subsequently, systemic toxicity was evaluated by testing biochemical indexes. As displayed in Fig. S11a (Supporting information), liver biochemical parameters, including aspartate aminotransferase (AST), alanine aminotransferase (ALT), alkaline phosphatase (ALP) and glutamyl transferase (GGT) were detected and

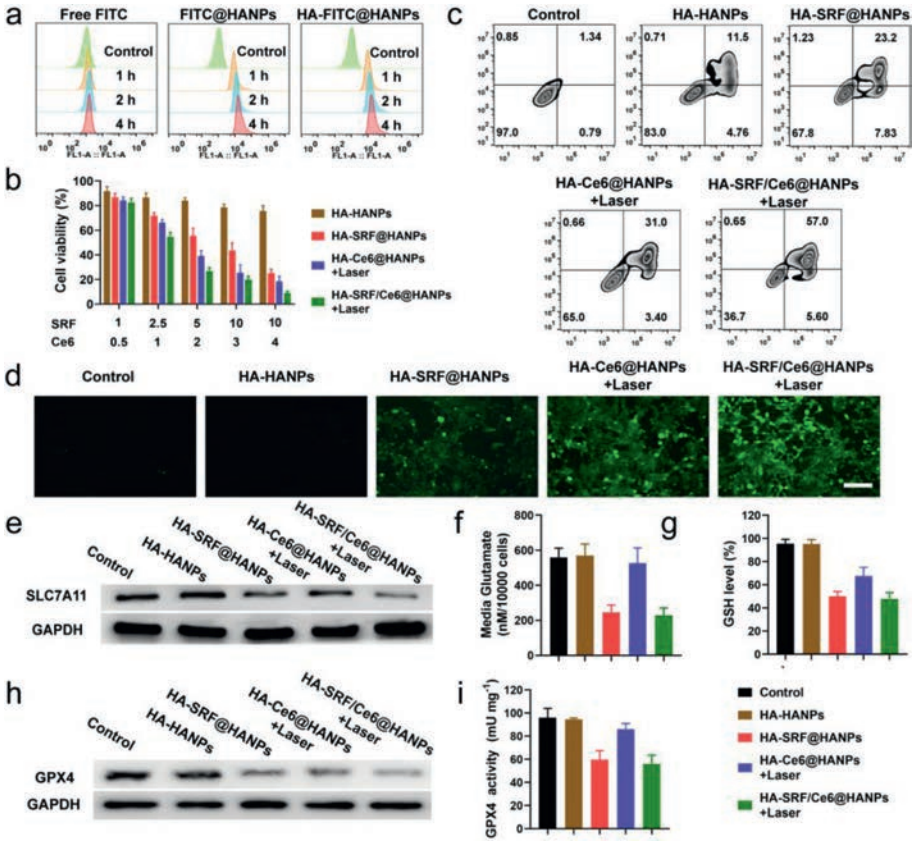

Fig. 2. (a) Cell uptake. (b) Cell viability. (c) Cell apoptosis experiment. (d) Intracellular ROS detection, scale bar: 200 μm. (e) SLC7A11 expression level. (f) Glutamate release. (g) Intracellular GSH level. (h) Western blot results for GPX4 expression. (i) GPX4 activity. GAPDH, glyceraldehyde-3-phosphate dehydrogenase.

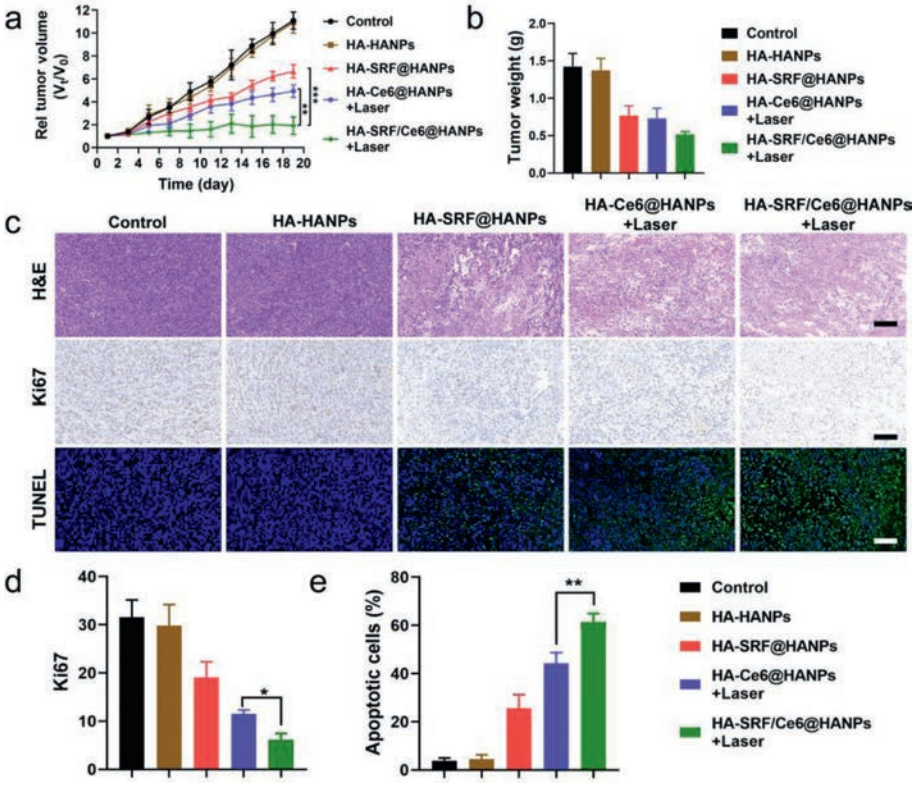

Fig. 3. (a) Relative tumor volumes ($n = 5$). (b) Tumor weight in different treatment groups ($n = 5$). (c) H&E, Ki67 and TUNEL staining of the tumor tissues, scale bar: 200 μm. (d) Ki67 and (e) TUNEL and positive tumor cells ($n = 3$). Data represent means ± standard deviation (SD), statistical analysis by one-way analysis of variance (ANOVA). $^{*}P < 0.05$, $^{**}P < 0.01$, $^{***}P < 0.001$.

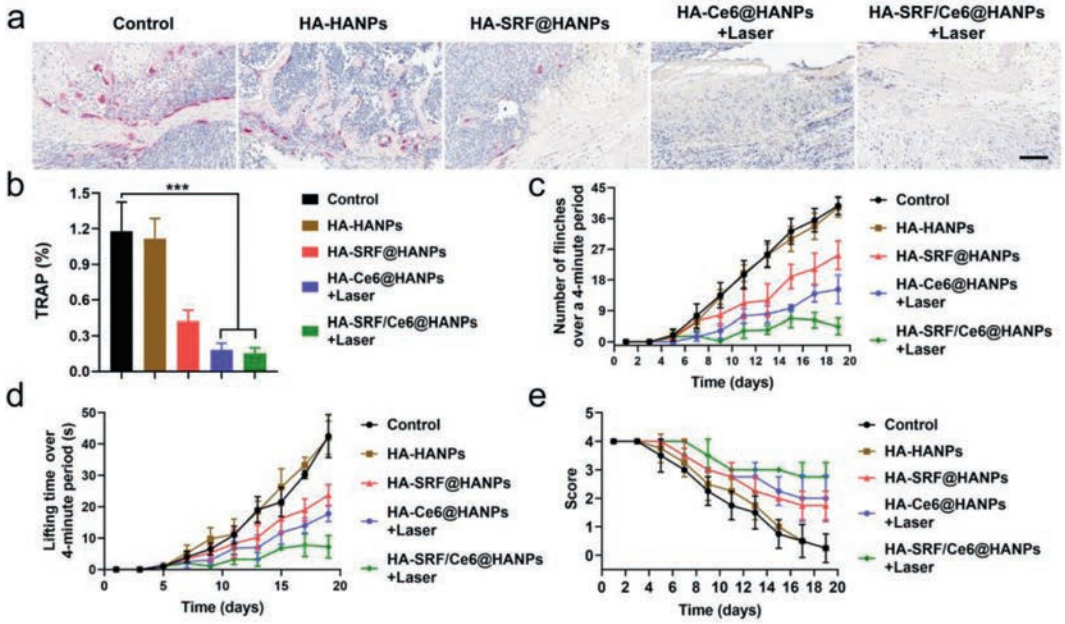

Fig. 4. (a, b) TRAP staining of the tumor tissues. Scale bar: 200 μm. (c) Number of flinches. (d) Spontaneous lifting time and (e) score of bone metastatic hindlimb. Data represent means ± SD ($n = 5$). $^{***}P < 0.001$.

all of these parameters were within the normal range. Kidney biochemical parameters (Fig. S11b in Supporting information), such as blood urea nitrogen (UREA), creatinine (CREA) and uric acid (UA) of all treatment groups showed no significant differences compared with control group. These results indicated that this therapeutic strategy showed negligible damage on renal and hepatic functions. Moreover, neither obvious body weight drop (Fig. S12 in Supporting information) nor abnormality in main tissue sections (Fig. S13 in Supporting information) were observed in all treatment groups at the end of antitumor studies. Overall, the hematology and histopathology analysis demonstrated that HA-SRF/Ce6@HANPs possessed superior biocompatibility *in vivo*.

In this current study, we focused our eyes on the concurrent treatment of breast cancer bone metastasis and CIBP. The nanoplatform boosted PDT *via* the synergism of SRF-mediated interruption of system SLA7A11/GSH/GPX4 antioxidant axis and Ce6-induced ROS storm, which were verified by *in vitro* and *in vivo* experiments. Next, HA-SRF/Ce6@HANPs exhibited excellent analgesic effect, which was mainly attributed to reduced levels of extracellular glutamate in the bone metastases microenvironment and suppression of tumor growth and metastasis. As expect, the combination of PDT and SLC7A11 inhibition exhibited encouraging performance in both tumor suppression and pain management, which was demonstrated in mice model of breast cancer bone metastasis. Looking forward, whether other mechanisms in contained in the analgesic effect of HA-SRF/Ce6@HANPs+Laser deserve more in-depth investigation.

Declaration of competing interest

The authors declare that they have no known competing financial interests or personal relationships that could have appeared to influence the work reported in this paper.

Acknowledgments

This project was financially supported by the National Natural Science Foundation of China (No. 82001189), The Project Tackling of Key Scientific and Technical Problems of Henan Provine (No. 232102311163).

Supplementary materials

Supplementary material associated with this article can be found, in the online version, at doi:10.1016/j.cclet.2023.108506.

References

[1] R.L. Siegel, K.D. Miller, A. Jemal, CA Cancer J. Clin. 70 (2020) 7–30.
[2] R.E. Coleman, P.I. Croucher, A.R. Padhani, et al., Nat. Rev. Dis. Primers 6 (2020) 83–108.
[3] Y. Gao, I. Bado, H. Wang, et al., Dev. Cell 49 (2019) 375–391.
[4] Y. Huang, Z. Xiao, Z. Guan, et al., Acta Pharm. Sin. B 10 (2020) 2384–2403.
[5] X.Y. Ouyang, C. Yang, Z. Zhu, et al., Acta Physiol. Sin. 71 (2019) 343–349.
[6] C. Yang, Y. Sun, X. Ouyang, et al., Pain Med. 21 (2020) 3443–3450.
[7] J. Li, Y. Sun, G. Ding, et al., Biochem. Biophys. Res. Commun. 495 (2018) 2432–2438.
[8] J. Feng, S. Lepetre-Mouelhi, A. Gautier, et al., Sci. Adv. 5 (2019) eaau5148.
[9] R.G. Ungard, K. Linher-Melville, M. Nashed, et al., Mol. Pain 15 (2019) 1744806918822185.
[10] K.N. Theken, Prostaglandins Other Lipid Mediat. 139 (2018) 63–70.
[11] A.P. Bloom, J.M. Jimenez-Andrade, R.N. Taylor, et al., J. Pain 12 (2011) 698–711.
[12] N. Massaly, J. Temp, H. Machelska, et al., Pain 161 (2020) 2798–2804.
[13] V. Sindhi, M. Erdek, Pain Manag. 9 (2019) 307–315.
[14] R.G. Ungard, E.P. Seidlitz, G. Singh, Pain 155 (2014) 28–36.
[15] C. Liu, L. Zhou, L. Xie, et al., Chin. Chem. Lett. 33 (2022) 2537–2540.
[16] H.M. Ellingson, T.W. Vanderah, Curr. Opin. Supp. Pall. Care 14 (2020) 107–111.
[17] R. Zajaczkowska, M. Kocot-Kepska, W. Leppert, et al., Int. J. Mol. Sci. 20 (2019) 6047.
[18] G. Lu, X. Gao, H. Zhang, et al., Chin. Chem. Lett. 33 (2022) 1923–1926.
[19] Y. Lin, X. Chen, C. Yu, et al., Acta Biomater. 159 (2023) 300–311.
[20] Y. An, J. Zhu, F. Liu, et al., ACS Appl. Mater. Interfaces 11 (2019) 29655–29666.
[21] H. Lv, S. Ma, Z. Wang, et al., Chin. Chem. Lett. 32 (2021) 1765–1769.
[22] P. Koppula, L. Zhuang, B. Gan, Protein Cell 12 (2020) 599–620.
[23] S.J. Dixon, D.N. Patel, M. Welsch, et al., Elife 3 (2014) e02523.
[24] L.S. Lin, T. Huang, J. Song, et al., J. Am. Chem. Soc. 141 (2019) 9937–9945.
[25] X. Meng, J. Deng, F. Liu, et al., Nano Lett. 19 (2019) 7866–7876.
[26] T. Liu, L. Jiang, O. Tavana, et al., Cancer Res. 79 (2019) 1913–1924.
[27] J.L. Parker, J.C. Deme, D. Kolokouris, et al., Nat. Commun. 12 (2021) 7147.
[28] F. Jiang, C. Yang, B. Ding, et al., Chin. Chem. Lett. 33 (2022) 2959–2964.
[29] Q. Song, J. Jia, X. Niu, et al., Nanoscale 11 (2019) 15958–15970.
[30] Y. Qiu, X. Xu, W. Guo, et al., ACS Biomater. Sci. Eng. 6 (2020) 2323–2335.
[31] E. Sistanipour, A. Meshkini, H. Oveisi, Colloids Surf. B: Biointerfaces 169 (2018) 329–339.
[32] X. Sun, X. Niu, R. Chen, et al., Hepatology 64 (2016) 488–500.
[33] W. Meng, M.M. Hao, N. Yu, et al., Mol. Pain 15 (2019) 1744806919871813.
[34] F. Wang, L. Chen, R. Zhang, et al., J. Control. Release 196 (2014) 222–233.
[35] Y. He, Y. Huang, Z. Huang, et al., J. Control. Release 264 (2017) 76–88.